

Supplementary Material

A. Effect of Diffeomorphism on Registration

In this study, LogDemons [1] is employed as the base registration model due to its capability to estimate an initial diffeomorphic displacement field, which aligns well with the characteristics of liver diffeomorphic deformation. In Fig. 1, we qualitatively evaluate the influence on the estimated displacement field and the warped image when employing classic Demons [2] without diffeomorphic constraint as the base registration model. The Demons-based and LogDemons-based models register the pre-MWA image (Fig. 1[a]) to post-MWA image (Fig. 1[d]). With the use of the same parameters, the Demons-based model estimates deformation field that exhibits discontinuous deformations (Fig. 1[b]), primarily due to the absence of diffeomorphic constraint. These discontinuous deformations introduce distortions in the image (Fig. 1[e]), which significantly impact the accuracy of the registration process. As a consequence, the Helmholtz decomposition is unable to effectively quantify tissue shrinkage, resulting in a degradation of the registration accuracy, especially in the tumor region. By employing diffeomorphic constraint, the LogDemons-based model avoids the discontinuous deformations and provides a more continuous and realistic deformation field (Fig. 1[c]). The smoothness of the deformation field facilitates the Helmholtz decomposition to effectively quantify tissue shrinkage, allowing for better compensation and registration accuracy in both liver and tumor regions (Fig. 1[f]).

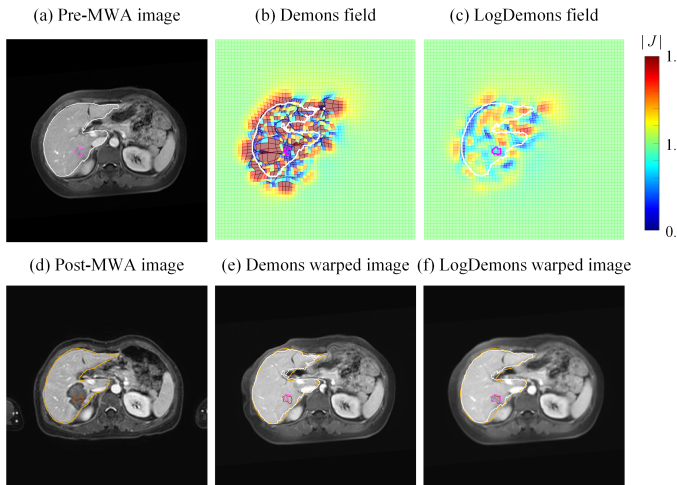


Fig. 1. Displacement fields and warped results of Demons and LogDemons as the base registration models. The first column depicts the moving image (a) and the fixed image (d) with white and orange contours representing the livers, and pink and brown contours indicating the tumors. The subsequent columns display the displacement fields and their corresponding warped results for each base model. The displacement fields are visualized as warped grids with colors indicating the Jacobian determinant values.

B. Implementation and Parameters

We implement our LC-BM method based on the open-source implementation of LogDemons [1] using Insight Toolkit, SimpleITK, Visualization Toolkit, and ArrayFire GPU matrix library. Table I shows the detailed parameters of LC-BM.

TABLE I
LIST OF THE PARAMETERS FOR LC-BM METHOD

Parameters for registration and finite difference solution			
Parameter	Value	Description	Type
j	3	Multi-resolution	Registration
i	100	Maximum number of iterations at each resolution	Registration
σ_v	3	Gaussian kernel for smoothing v	Registration
σ_u	4	Gaussian kernel for smoothing u	Registration
n	3000	Maximum number of iterations	FD solution

Parameters for tissue properties			
Parameter	Value	Unit	Reference
k	0.564	$\text{W} \cdot (\text{m} \cdot \text{K})^{-1}$	[3]
ρ_b	1025	$\text{kg} \cdot \text{m}^{-3}$	[3]
c_b	3639	$\text{J} \cdot \text{kg}^{-1} \cdot \text{K}^{-1}$	[3]
ω_b	3.6×10^{-3}	$\text{kg} \cdot \text{m}^{-3} \cdot \text{s}^{-1}$	[3]
T_a	291.75	K	[4]
T_b	310.15	K	[4]
T_c	333.15	K	[3]
E	4500	Pa	[4]
ν	0.45		[4]
λ	3×10^{-4}		[4]

Parameters for SAR (forward side without water cooling, when $z \geq 0$)						
$P(W)$	α	β	c_0	c_1	c_2	c_3
40	4.818	-4.623	0.1755	-0.5024	-1.68	4.628
45	2.668	-3.896	0.1349	-0.5342	-0.9628	4.132
50	2.612	-3.633	0.0638	-0.1692	-0.9078	2.548
55	3.482	-3.831	0.2059	-0.9425	-0.3111	3.827
60	5.512	-4.845	0.1669	-0.2927	-2.817	6.389

Parameters for SAR (forward side without water cooling, when $z < 0$)						
$P(W)$	α	β	c_0	c_1	c_2	c_3
40	4.818	-4.623	0.2382	-1.39	0.5897	4.628
45	2.668	-3.896	0.0671	-0.769	0.8524	4.132
50	2.612	-3.633	0.0019	-0.4213	0.8943	2.548
55	3.482	-3.831	0.1721	-0.898	-0.0862	3.827
60	5.512	-4.845	0.2137	-1.707	1.6760	6.389

C. Baseline Characteristics

Table II shows the baseline characteristics of patients. The tumors in these patients are 31 for hepatocellular carcinoma and 16 for other types (including 1 for focal nodular hyperplasia, 2 for intrahepatic cholangiocarcinoma, 2 for hepatic

hemangioma, 11 for metastatic cancer). All tumors in this study were histologically confirmed by biopsy. The volume of each tumor is shown in Fig. 2. Overall, the mean volume of the tumors is 2.74 mL (range, 0.12–14.95 mL).

TABLE II
PATIENT CHARACTERISTICS

	Category	Number of patients	Ratio of patients (%)
Age at inclusion	< 55	9	25
	≥ 55	27	75
Sex	Male	31	86
	Female	5	14
Cirrhosis	Present	22	61
	Absent	14	39
Child-Pugh class	A	36	100
	Others	0	0
Number of tumors	1	26	72
	2	9	25
	3	1	3
Cause	Hepatitis B virus	16	44
	Hepatitis C virus	3	9
	Alcohol	1	3
	Others	16	44

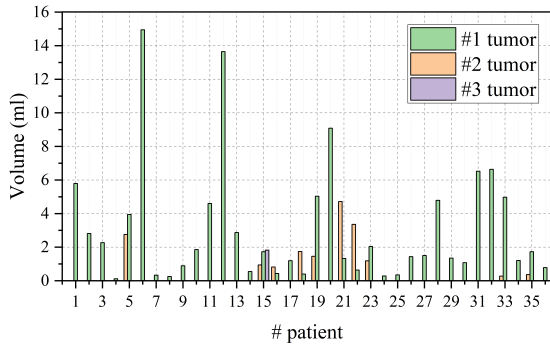


Fig. 2. The volume of each tumor. Multiple tumors of the same patient are represented in green, orange and purple, respectively.

D. Representative Results

Fig. 3 shows the difference in the nature of the displacement fields estimated by the different methods and how it affects the accuracy of the registration. Comparing the fixed and moving images, we can find that the liver has large-scale deformation, and the tumor in the moving image has similar texture to the coagulation in the fixed image, which could lead to incorrect match. The warped images by each method are shown in the first and third rows of Fig. 3, where the warped liver and tumor contours with exclusive colors are overlaid on the warped image. The estimated displacement fields by each method are presented in warped grids below their corresponding warped images (second and fourth rows of Fig. 3). Jacobian determinants (Jacobi) are mapped onto the grid, tending to blue for shrinkage, to red for expansion, and to green for incompressibility. To tackle the incorrect match, the methods of Kim and Fu use local incompressibility constraint where the deformation at the tumor is restricted to be incompressible, which can be observed that the Jacobi inside the tumor region tends to green. Incompressible deformation keeps the tumor

volume constant and thus reduces incorrect match, but this in turn does not compensate for tissue shrinkage, making the registration accuracy of the tumor decrease. In addition, Kim's method models the displacement field as a viscous fluid and can only use small optimization step in the registration, resulting in the inability to compensate for the large-scale deformation of the liver. Rieder's method avoids incorrect match by estimating a rigid transformation based on ROI regions of coagulation and tumor. Unlike Rieder's method, Luu's method restricts the local rigidity of the deformation in the tumor region to mitigate incorrect match, as seen by Jacobi near the tumor tends to green. However, the rigid transformation cannot compensate for nonrigid deformation of tumor, resulting in a low registration accuracy of the tumor. Moreover, the rigid transformation estimated by Rieder's method is based on the ROI regions only and ignores the deformation of the liver, which also leads to low registration accuracy of the liver. Solbiati's method performs an unrestricted nonrigid registration. We can find Jacobi tends to red in the tumor region, indicating an increase in the volume of the tumor due to the incorrect matching toward the coagulation. This phenomenon can be also observed in some unconstrained deep learning-based methods (VoxelMorph, HyperMorph and SegisNet), which leads to a decrease in the registration accuracy of the tumor. Liu's method uses a local contractive nonrigid registration to quantify the tissue shrinkage, which improves the registration accuracy of the tumor. However, tissue shrinkage is modeled entirely by field analysis and does not take into account biomechanical properties in Liu's method, which makes the degree of contraction of tumors highly influenced by the liver surface. LapIRN utilize a multi-resolution strategy and pyramid similarity metric to estimate the displacement field, which helps to avoid local minima and to estimate a smooth displacement field. However, the registration accuracy of the tumor is limited by the lack of tissue shrinkage compensation. SynthMorph uses randomly generated homogeneous synthetic images to train the network. This registration model has difficulty in correctly estimating deformation in the region with inconsistent appearance, resulting in lower tumor registration accuracy. By using LC-part, LC-BM can decompose the multi-source motions and correct the respiratory motion individually, thereby obtaining a highly accurate liver alignment. In addition, given the BM-part, LC-BM is able to compensate for tissue shrinkage, and the warped tumor is highly aligned with the ground truth.

After registration, the location of the residual tumor can be indicated by comparing the warped tumor to the coagulation. Fig. 4 shows the location of the residual tumor indicated by different methods. In the case of complete ablation (subject1 in Fig. 4), the tumor is completely enclosed by coagulation, so no residual tumor is present. False alarm of residual tumor may increase the workload of physicians or lead to unnecessary treatment of the patient. As shown in Fig. 4, LC-BM, Luu and SynthMorph indicate no residual tumor, whereas other methods incorrectly indicate the presence of residual tumor. In the case of incomplete ablation (subject2 in Fig. 4), the residual tumor indicated by LC-BM is highly consistent with the ground truth, whereas the methods of Kim,

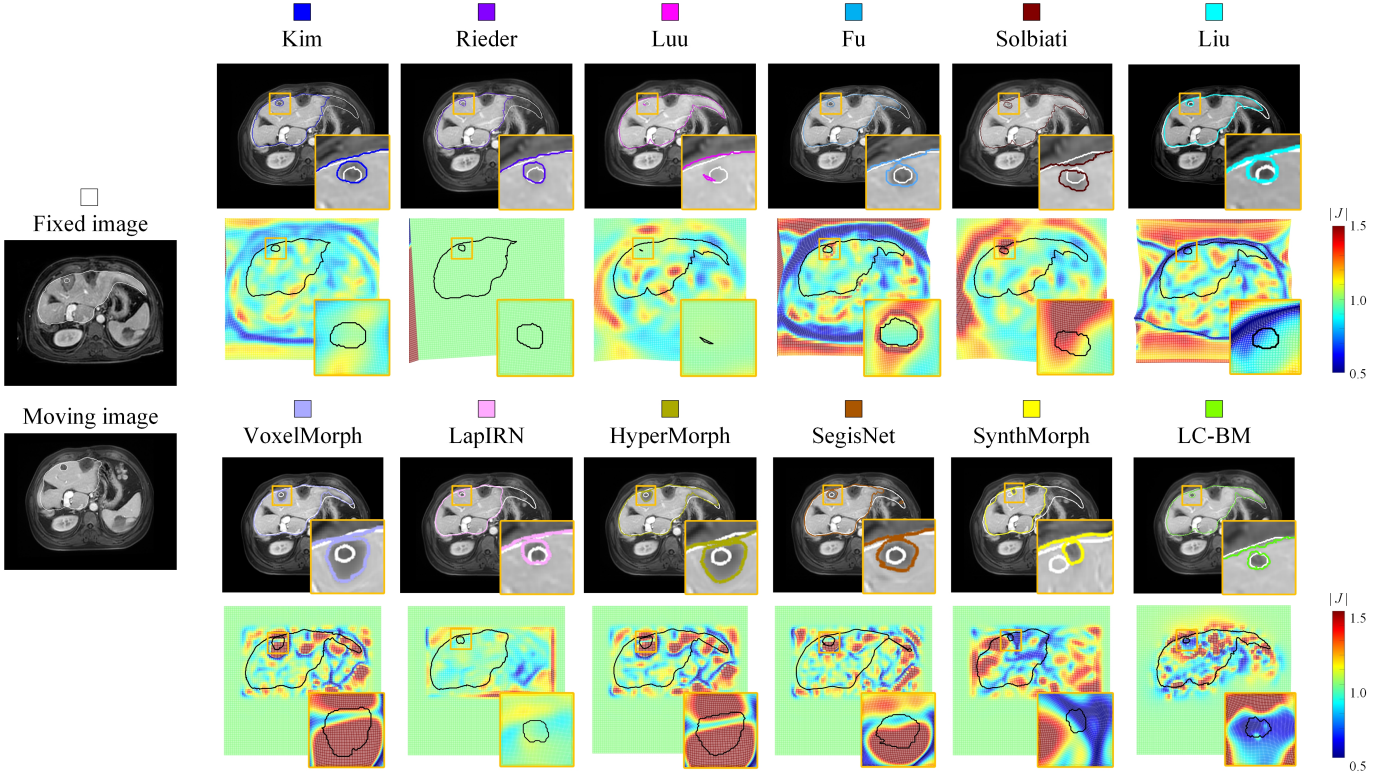


Fig. 3. Displacement fields and warped results of different methods. The first column is the fixed image and the moving image with white contours indicating the liver and the tumor. The subsequent columns show the warped results (first and third rows) and the corresponding displacement fields (second and fourth rows) for each method. The displacement fields are shown as warped grids with Jacobian determinant colors. When the Jacobian determinant is greater than 1, the grid tends to be red, which indicates that the local volume increases. Conversely, a decrease in local volume is indicated when the grid tends to be blue. Note that warped liver and tumor of each method are indicated by contours of corresponding color, whereas black contours are used in displacement field for easy observation.

Luu, Fu, Solbiati, Liu, VoxelMorph, LapIRN and SynthMorph do not indicate the presence of residual tumor. In addition, the methods of Rieder, HyperMorph and SegisNet indicate incorrect locations of residual tumor. Missing alarm or incorrect indication of residual tumor may result in patients not receiving timely supplemental treatment. Considering that LC-BM quantifies and compensates for tissue shrinkage, the warped tumor is highly aligned with the ground truth, thereby correctly indicating the location of residual tumor, on which physicians could decide whether to proceed with supplemental treatment.

E. Risk Factors of Local Tumor Progression

We analyze the risk factors of the local tumor progression (LTP) for the incomplete ablation cases (MAM below 0 mm). The location and MFD of the tumors in these cases are shown in Fig. 5. Recent studies [5], [6] have reported that the location and size of the liver tumor are the risk factors of the LTP after ultrasound-guided MWA. In Fig. 5, we find that all tumors are in challenging locations [6], [7] (#1–3, 5–8, and 10–13 are located at the liver margin, where complete ablation would injure the adjacent organs; #3–7, 9, and 12–13 are near the blood vessel). In addition, #4–7, 9, and 13 have large tumors ($MFD > 3$ cm).

F. Relative Volume Changes of Coagulations and Tumors

We count the relative volume changes of coagulations and tumors in all cases after tissue shrinkage compensation by LC-BM, as shown in Fig. 6. The relative volume change for all coagulations is greater than 0, which indicates that the coagulations size after compensation is larger than the previous size, meaning that the coagulation dimension is underestimated. This phenomenon is consistent with the results in clinical trial [8], which found that the actual coagulations size is larger than the visualized size. It is easy to understand that tissue shrinkage can lead to an underestimation of coagulation size, and conversely, we may intuitively think that the tumor will shrink. However, we find an interesting phenomenon that the tumor volume may increase in some cases as shown in Fig. 6(b).

We first analyze the causes of tumor volume shrinkage and expansion by using a simulation example and then show two representative cases of clinical data for both phenomenon (Fig. 7). In the simulation example, we create a simple contraction field that contracts toward the center. Jacobi are mapped onto the grid, tending to blue for shrinkage, to red for expansion, and to green for incompressibility. We can find that the central region is locally contracted, whereas the peripheral region is locally expanded. Then, we generate two tumors (white and black dashed lines) in the central and peripheral regions and

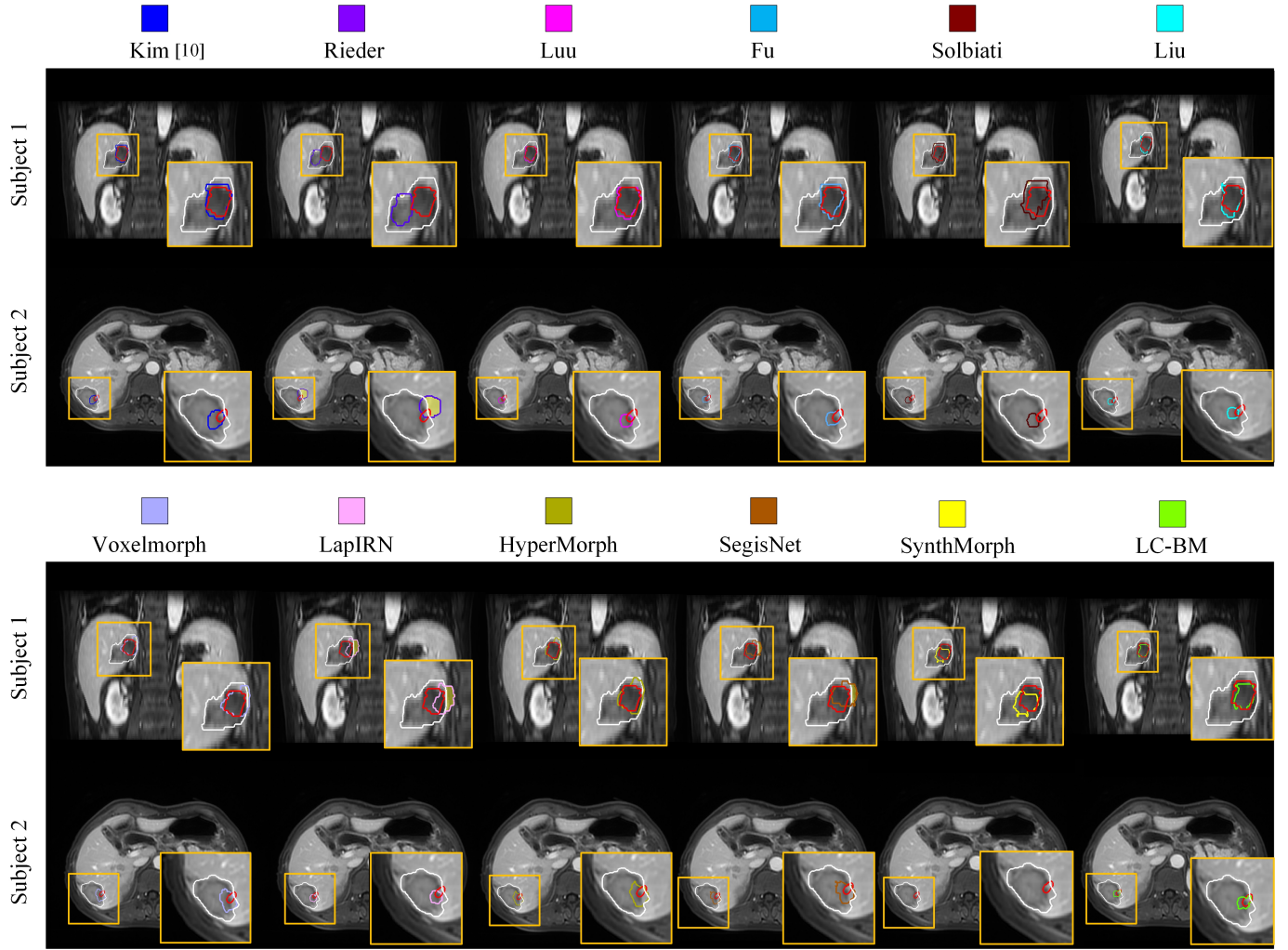


Fig. 4. Location of the residual tumor indicated by different methods. The white and red contour lines are the coagulation and ground-truth tumor, respectively, and the contour lines of other colors are the warped tumors of different methods. The area where the red contour line runs out the white contour line is considered as the ground truth for residual tumor. The yellow-highlighted areas are the location of the residual tumors indicated by different methods. Subject1 is the case of complete ablation; thus, no residual tumor should be found. Conversely, subject2 is the case of incomplete ablation; thus, the indicated residual tumor should match the location of the ground-truth residual tumor as much as possible.

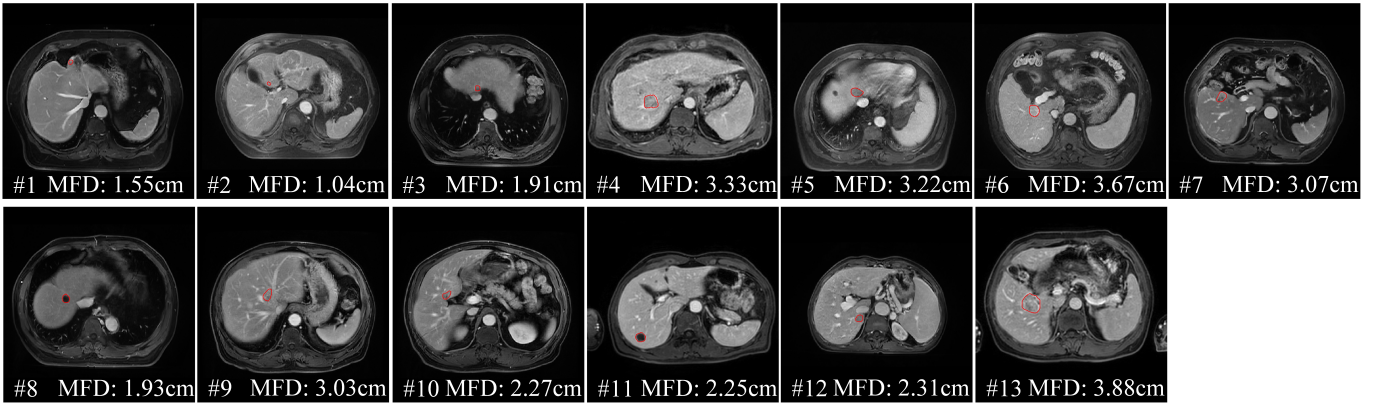


Fig. 5. Location and MFD of tumors in incomplete ablation cases. Red contour lines represent the tumors.

observe the volume change after deformation (white and black solid lines). The tumor located at the center contracts, whereas the tumor at the periphery expands, suggesting that the position of the tumor in the contraction field affects the trend of its

volume change. Essentially, if the MWA applicator is mis-localized and placed in a position near the tumor, the process of local region contraction could potentially produce local stretching in neighboring regions. This situation could result in

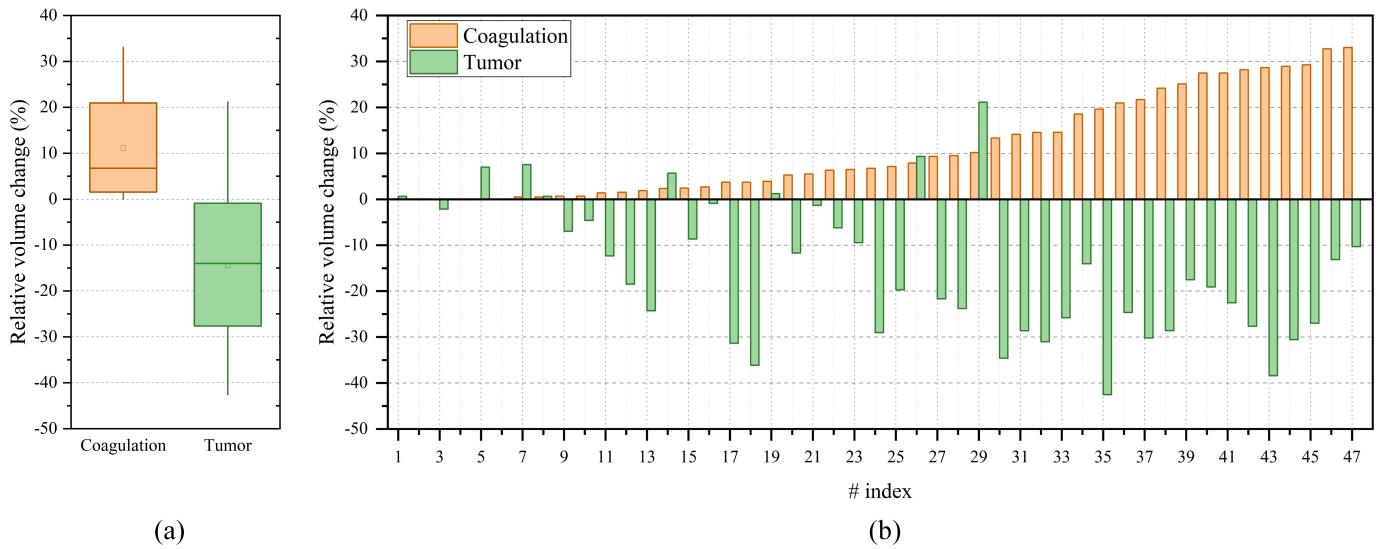


Fig. 6. The relative volume change of coagulation and tumor after compensation by the proposed method in all cases.

a nearby tumor experiencing an expansion and thus potentially increasing its imaging volume signature. This assumption is confirmed by the cases of shrinkage and expansion in clinical data. We show two representative cases in Fig. 7. This phenomenon illustrates the effect that different locations of the applicator could exert on the tumor. This effect should be considered not only during the post-MWA assessment but also during the planning of MWA.

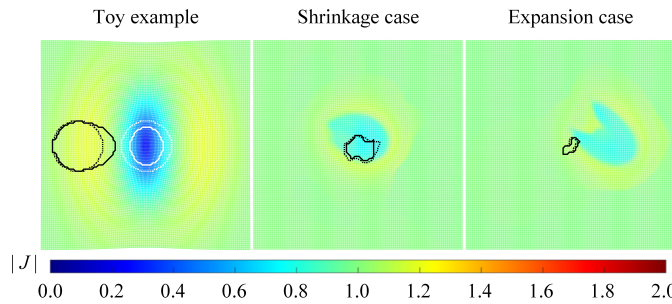


Fig. 7. Different tumor positions in a contraction field may result in volume shrinkage or expansion. The contraction fields are shown as warped grids with Jacobian determinant colors. In the simulation example, we use white and black lines to represent shrinking and expanding tumors, respectively. For the shrinkage and expansion cases in the clinical data, we use uniformly black lines to represent tumors for easy observation.

REFERENCES

- [1] T. Vercauteren, X. Pennec, A. Perchant, and N. Ayache, "Symmetric log-domain diffeomorphic registration: A demons-based approach," in *Medical Image Computing and Computer Assisted Intervention*, vol. 5241. Springer, 2008, pp. 754–761.
- [2] J.-P. Thirion, "Image matching as a diffusion process: an analogy with maxwell's demons," *Medical image analysis*, vol. 2, no. 3, pp. 243–260, 1998.
- [3] C. L. Brace, "Radiofrequency and microwave ablation of the liver, lung, kidney, and bone: what are the differences?" *Current problems in diagnostic radiology*, vol. 38, no. 3, pp. 135–143, 2009.

- [4] C. S. Park, C. Liu, S. K. Hall, and S. J. Payne, "A thermoelastic deformation model of tissue contraction during thermal ablation," *International Journal of Hyperthermia*, vol. 34, no. 3, pp. 221–228, 2018.
- [5] J. Yu, P. Liang, X.-l. Yu, Z.-g. Cheng, Z.-y. Han, M.-j. Mu, Q.-y. Li, and Y.-m. Liu, "Local tumour progression after ultrasound-guided microwave ablation of liver malignancies: risk factors analysis of 2529 tumours," *European radiology*, vol. 25, pp. 1119–1126, 2015.
- [6] C. An, Z. Cheng, X. Yu, Z. Han, F. Liu, X. Li, S. S. Wu, J. Yu, and P. Liang, "Ultrasound-guided percutaneous microwave ablation of hepatocellular carcinoma in challenging locations: oncologic outcomes and advanced assistive technology," *International Journal of Hyperthermia*, vol. 37, no. 1, pp. 89–100, 2020.
- [7] J. S. Kim, W. Kim, Y. H. So, S. J. Yu, and B. G. Kim, "Topographical impact of hepatitis b-related hepatocellular carcinoma on local recurrence after radiofrequency ablation," *Journal of Clinical Gastroenterology*, vol. 48, no. 1, pp. 66–72, 2014.
- [8] D. Liu and C. L. Brace, "Evaluation of tissue deformation during radiofrequency and microwave ablation procedures: Influence of output energy delivery," *Medical physics*, vol. 46, no. 9, pp. 4127–4134, 2019.